Supplementary Material for "Plug-and-Play Approach to Non-adiabatic Geometric Quantum Computation"

Bao-Jie Liu,[1] Xue-Ke Song,[1] Zheng-Yuan Xue,[2,1,*] Xin Wang,[3,†] and Man-Hong Yung[1,4,5,‡]

[1]*Institute for Quantum Science and Engineering, and Department of Physics, Southern University of Science and Technology, Shenzhen 518055, China*
[2]*Guangdong Provincial Key Lab Recompile 29 oratory of Quantum Engineering and Quantum Materials, GPETR Center for Quantum Precision Measurement, and SPTE, South China Normal University, Guangzhou 510006, China*
[3]*Department of Physics, City University of Hong Kong, Tat Chee Avenue, Kowloon, Hong Kong SAR, China, and City University of Hong Kong Shenzhen Research Institute, Shenzhen, Guangdong 518057, China*
[4]*Shenzhen Key Laboratory of Quantum Science and Engineering, Shenzhen 518055, China*
[5]*Central Research Institute, Huawei Technologies, Shenzhen 518129, China*

(Dated: August 20, 2019)

I. COMPARISON WITH VARIOUS GEOMETRIC QUANTUM COMPUTATIONS

To illustrate how we deviate from the traditional treatments of GQC, we shall succinctly derive various forms of GQCs in the *same* framework; the goal is to provide a unified view on GQC, connecting all of the different approaches together.

A. Abelian and Non-Abelian Adiabatic GQC

Let us first consider the diagonal form of the time-dependent Hamiltonian $H(t)$, by the time-dependent basis $\{|e_k(t)\rangle\}$, i.e.,

$$H(t)=\sum_k E_k(t)\,|e_k(t)\rangle\langle e_k(t)|\,, \tag{1}$$

where $\{E_k(t)\}$ are the instantaneous eigenvalues of $H(t)$ at time t. In this case, we consider the auxiliary basis states $\{|\mu_m(t)\rangle\}$ to be identical to the eigenstates $\{|e_m(t)\rangle\}$ of $H(t)$. For simplicity, suppose the eigenvalues are non-degenerate, then we have,

$$\langle\mu_k(t)|\,H(t)\,|\mu_l(t)\rangle=\delta_{kl}E_k(t)\ . \tag{2}$$

Furthermore, the adiabatic theorem [1] suggests that there is no transition occurs when the variation of $H(t)$ is sufficiently slow, which implies that, $A_{kl}(t)=0$ whenever $k\neq l$. Consequently, after a cycle where $H(\tau)=H(0)$, the unitary transformation becomes an Abelian transformation [2], i.e.,

$$U(\tau)=\sum_k e^{i\varphi_k}\,|e_k(0)\rangle\langle e_k(0)|\,, \tag{3}$$

where $\varphi_k\equiv i\int_0^\tau\langle e_k(t)|\dot{e}_k(t)\rangle dt-\int_0^\tau E_k(t)dt$ is the sum of the geometric and dynamical phases.

Derivation of the results for non-Abelian GQC [3] is straightforward in this approach under the adiabatic approximation, where transition away from a degenerate subspace is not allowed. In this subspace, the Hamiltonian is diagonal in a certain basis, i.e.,

$$H_{\text{sub}}(t)\equiv E(t)\sum_k|e_k(t)\rangle\langle e_k(t)|\,. \tag{4}$$

TABLE I. Comparison with various approaches to geometric quantum computation

Schemes	AHQC[a]	NHQC[b]	NHQC+
Robust to systematic errors?	√	×	√
Robust to random errors?	√	√	√
Reduction of decoherence?	×	√	√
Extensible for optimization?	×	×	√
Gate time	long	short	short
References	[2, 3, 6–8]	[4, 5, 9–15]	this work

[a] AHQC: Adiabatic Holonomic quantum computation
[b] NHQC: Nonadiabatic Holonomic quantum computation

In this case, $H_{kl}(t)=\delta_{kl}E(t)$, and the vector potential no longer acting trivially in this subspace,

$$U(\tau)=e^{-i\int_0^\tau E(t)dt}\mathcal{T}e^{i\int_0^\tau A(t)dt}\,, \tag{5}$$

where $A(t)\equiv\sum_{kl}A_{kl}(t)\,|e_k(0)\rangle\langle e_l(0)|$. This forms the basis for constructing adiabatic geometric gates.

B. Nonadiabatic Holonomic Quantum Computation

We review NHQC (comparable with e.g. Ref. [4, 5]) using this language of general framework. First, we choose the auxiliary state to be proportional to the dynamical states, i.e.,

$$|\mu_m(t)\rangle\equiv e^{-if_m(t)}\,|\psi_m(t)\rangle\ , \tag{6}$$

where $f_m(t)$ is a phase angle satisfying $f_m(0)=0$. The basis vectors are chosen as

$$|\psi_m(t)\rangle=\sum_l c_{lm}e^{-i\int_0^t E_l(t')dt'}\,|e_l\rangle\ , \tag{7}$$

where $E_l(t)$ and $|e_l\rangle$ are the instantaneous eigenvalue and eigenstate of the Hamiltonian $H(t)$. Consequently, the effective Hamiltonian $H_{eff}(t)$ becomes diagonal, i.e., $A_{ml}(t)-H_{ml}(t)=\delta_{ml}\dot{f}_m(t)$, which implies that

$$U(\tau)=\sum_m e^{if_m(\tau)}\,|\psi_m(0)\rangle\langle\psi_m(0)|\,. \tag{8}$$

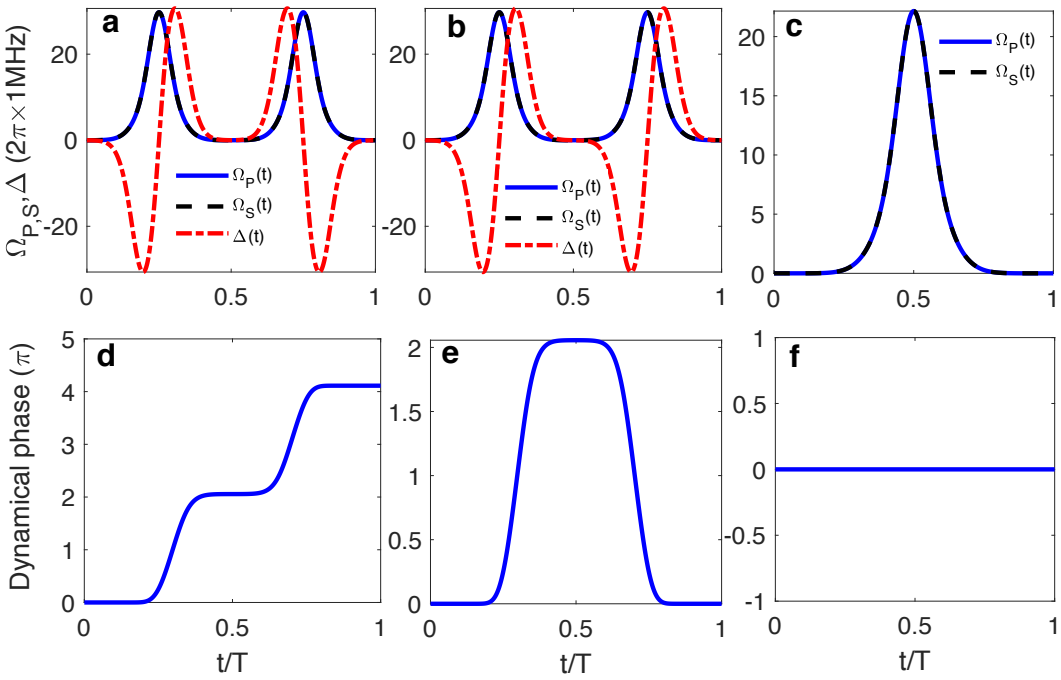

FIG. 1. Schematic diagram of the pulse shapes and dynamical phases. Pulse sequences corresponding to DG, NHQC+ and NHQC schemes for realizing the NOT gates are shown in (a), (b) and (c). Dynamical phases of DG, NHQC+ and NHQC with (d), (e) and (f) as a function of time t (unit of T) in whole evolution.

The point is that $f_m(\tau)$ represents an overall phase, including both dynamical phase and geometrical phase. In order to obtain a pure geometric gate, an additional constraint is often imposed for NHQC [4, 5]: for *all* j and k, and at *all* times t,

$$\langle\psi_m(t)|\, H(t)\, |\psi_k(t)\rangle = 0\,, \tag{9}$$

which means that, at least for a certain subspace, the Hamiltonian acts as a null matrix, and represents a rather strong restriction for the choice of the time-evolution Hamiltonian and weaken the noise robustness. Our work aims to relax such a condition.

C. Proof of Theorem 1

For a general time-dependent Hamiltonian $H(t)$, here, we move the Hamiltonian $H(t)$ to effective Hamiltonian $H_{eff}(t)$ with $V(t) = \sum_k |\mu_k(t)\rangle\langle\mu_k(0)|$, where related unitary is $V(t)$ maps the time-dependent vectors $|\mu(t)\rangle$ onto the time-independent state $|\mu(0)\rangle$ all the time.

Proof. According to the initial condition that von Neumann equation Eq. (7) is satisfied in main text, we take an identical transformation as

$$iV^\dagger\frac{\partial\Pi_k(t)}{\partial t}V = [V^\dagger H(t)V, V^\dagger\Pi_k(t)V]\,, \tag{10}$$

It is easily found that

$$iV^\dagger\frac{\partial\Pi_k(t)}{\partial t}V(t) = i\frac{\partial(V^\dagger\Pi_k(t)V)}{\partial t} - i\frac{\partial V^\dagger}{\partial t}\Pi_k(t)V - iV^\dagger\Pi_k(t)\frac{\partial V}{\partial t}\,, \tag{11}$$

and

$$i\frac{(\partial V^\dagger V)}{\partial t} = i\frac{\partial V^\dagger}{\partial t}V + iV^\dagger\frac{\partial V}{\partial t} = 0\,. \tag{12}$$

Combining Eq. (12) and (11) with Eq. (10), we get,

$$\frac{\partial V^\dagger\Pi_k(t)V}{\partial t} = -i[V^\dagger H(t)V - iV^\dagger\dot{V}, V^\dagger\Pi_k(t)V)]\,. \tag{13}$$

Taking $\Pi_k(0) = V^\dagger\Pi_k(t)V$ into above equation, the Eq. (13) reduces to

$$[\Pi_k(0), H_{eff}(t)] = 0\,. \tag{14}$$

From the Eq. (14), we can clearly conclude that $\Pi_k(0)$ and $H_{eff}(t)$ are commutative. Thus, based on the result, we have the following equation as

$$\Pi_k(0)H_{eff}(t)\Pi_m(0) = 0, m \neq k \tag{15}$$

in other words

$$\langle\mu_m(0)\,|H_{eff}(t)|\mu_k(0)\rangle = 0, m \neq k. \tag{16}$$

The Eq. (16) has the same form as the Eq. (3) in the main text.

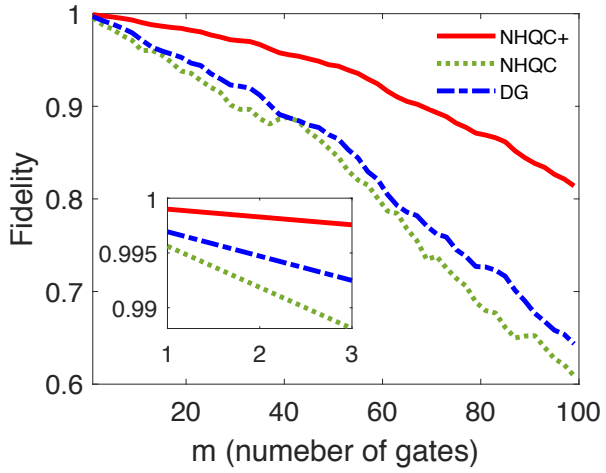

FIG. 2. Schematic diagram of the pulse shapes and dynamical phases. Pulse sequences corresponding to DG, NHQC+ and NHQC schemes for realizing the NOT gates are shown in (a), (b) and (c). Dynamical phases of DG, NHQC+ and NHQC with (d), (e) and (f) as a function of time t (unit of T) in whole evolution.

The NHQC+ approach, based on Theorem 1, developed here shares the same advantages of NHQC over adiabatic GQC in speeding up the operation times of quantum gates. We make a comparison with various approaches to geometric quantum computation, as shown in the Table I. In terms of systematic errors, NHQC+ can become potentially more robust; this is due to fact that NHQC+ removes the limitation of the pulse shape. In addition, NHQC+ is compatible with many optimization techniques, which may further makes it robust to other types of noises. For the previous approaches [4, 5] of NHQC, there is a set of rather strict constraints imposed to the driving Hamiltonian, in order to ensure the dynamical phase to vanish all the time during the gate operations. Practically, one can only choose fixed pulses for NHQC. For NHQC+, however, the parameter paths are typically not unique, as we can choose from a family of solutions. Consequently, we can design pulse sequences using optimal control theory to increase the robustness against different types of errors. Therefore, by removing the pulse-shape limitation of NHQC and being compatible with many existing optimization techniques, NHQC+ can become potentially more robust against different types of errors.

D. Robustness of NHQC+ vs NHQC and DG against random quasistatic noise

To show the noise-resilient feature of our NHQC+ gates, we take the quasistatic noise to compare the performance of our geometric gates with that of the corresponding DG and NHQC gates. Before that, we set the operation time of all the gates to be the same as $T = 2\tau = 180ns$, and the pulse shapes of DG and NHQC+ are set to with the Eq. (11) in main text but a spin-echo technique is applied to NHQC+ at time $t = \tau$ for canceling the accumulated dynamical phase in our simulation, as shown in the Fig. 1(a) and 1(b). The NOT gate of NHQC [4, 5] is realized by setting the parameters $\Delta = 0$ and $\Omega_{max}^{N} = 1.192\Omega_{max}$, where the Ω_{max} is the peak Rabi frequecy of NHQC+, so the operation time of NHQC is the same as NHQC+ as shown in 1(c). Meanwhile, we plot the dynamical phases of DG, NHQC+ and NHQC during a whole evolution as shown in Fig. 1(d), 1(e) and 1(f) to verfy the conditions of Eq. (5) in main text.

We have compared the fidelities with different gates against the different quasistatic stochastic constant noise β that fluctuate slowly compared with the system evolution during a single gate operation in main text. Here, we further illustrate the robustness of our NHQC+ aganist random quasistatic noises, where the random quasistatic noises $\beta(m) \in [-0.05, 0.05]$ is a function of gate numbers m following the experimental set. Here we choose 100 NOT gates to benchmark the noise-resilient feature. In Fig. 2, we present our numerical simulation result for DG, NHQC+ and NHQC gates which shows that the NHQC+ gate are indeed more robust than DG and NHQC gates to the random quasistatic noises. Meanwhile, we find that the NHQC gate are more sensitive to the random noises than DG due to the its fixed pulse area 2π.

F. The robustness comparison of NHQC+ and dynamical gates with optimal control

He, we further compare the robustness of our NHQC+ gates with that of the dynamical gates with optimal control. We first calculate both geometric and dynamical phases which are used to implement geometric and dynamics gates, respectively. The dynamic phase can be directly calculated from its definition as [2],

$$\begin{aligned}\gamma_d &= \int_0^T \langle \mu_+(t)|H(t)|\mu_+(t)\rangle\, dt \\ &= \int_0^T \sqrt{\Omega^2 - \dot{\chi}^2 + \Delta^2}dt. \end{aligned} \tag{17}$$

Meanwhile, the geometric phase is defined by [11]

$$\begin{aligned}\gamma_g &= i\int_0^T \left\langle \tilde{\mu}_+(t)|\frac{d}{dt}|\tilde{\mu}_+(t)\right\rangle dt \\ &= \pi + \int_{\alpha(0)}^{\alpha(T)} \cos\chi d\alpha, \end{aligned} \tag{18}$$

where $|\tilde{\mu}_+(t)\rangle = e^{-if(t)}|\mu_+(t)\rangle$; when $f(T) - f(0) = \gamma_d + \gamma_g$, $|\tilde{\mu}_+(T)\rangle = |\tilde{\mu}_+(0)\rangle$, which leads to cyclical evolution. The nonadiabatic geometric phase can be regarded as a geometric phase associated with a closed curve in the projecting Hilbert space. Combining with the decoupled dark state $|\mu_0\rangle$, we can realize both the NHQC+ gates, Eq. (13) in the main text, and dynamical gates.

Here, we use the U_S gate with $\gamma = \frac{2\pi}{3}$, $\theta = -\arccos\frac{1}{\sqrt{3}}$, and $\phi = \frac{3\pi}{4}$ as a test gate. Specifically, we realize NHQC+

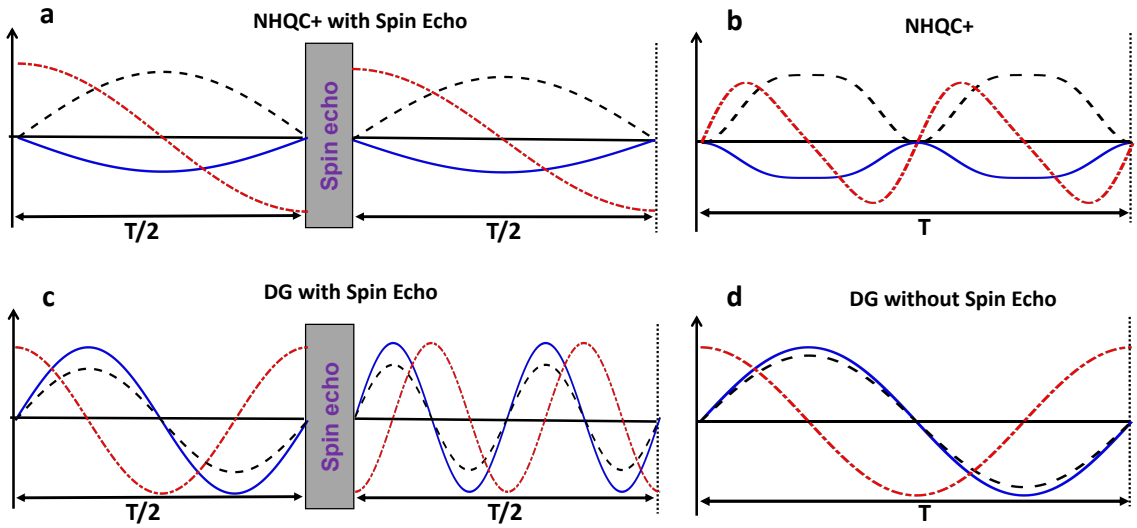

FIG. 3. Pulse shapes of different implementations for U_S gate: (a) NHQC+ Spin Echo, (b) NHQC+, (c) DG+ Spin Echo and (d) DG schemes, where the pulse shapes of Rabi frequency Ω_P, Ω_S and the detuning Δ are shown in solid blue line, dashed black line, and dotted dashed red line, respectively. The related parameters are shown in Table II.

gate and DG with and without spin echo, by choosing proper parameters to control the geometric and dynamical phases, and the pulse shapes of which are shown in Fig. 3. In particular, we also implement NHQC+ gate using the pulses-shaping method without spin echo to distinguish the robustness obtained from geometric operation and spin echo. To achieve this, we can simplify the implementation in the main text, by setting $\Delta(t) = \Omega_0 F(t)\cos\chi(t)$ and $\Omega(t) = \sqrt{\dot{\chi}^2(t) + (\Omega_0 F(t)\sin\chi(t))^2}$, where the dynamical phase $\gamma_d = \int_0^T \Omega_0 F(t)dt$ can be concealed by properly choosing the form of $F(t)$ during the gate implementation. For a simple choice, we set

$$F(t) = A\sin\frac{2\pi t}{T} + B\sin^3\frac{2\pi t}{T}, \tag{19}$$

where A=2 and B=-1 are chosen to ensure that the maximum Rabi amplitude here is the same as the other three pulses in NHQC+ Spin Echo and DG with and without spin echo schemes. The related parameters of all the above four pulse shapes are listed in Table II.

TABLE II. The parameters of the Eq. (8) and Eq. (11) in main text are chosen for various approaches to quantum gate.

Type	NHQC+SE [a]	NHQC+	DG+SE	DG
Ω_0 (MHz)	$2\pi\times10$	$2\pi\times10$	$2\pi\times8.88$	$2\pi\times8.88$
T (ns)	200	200	100	75
θ	$-\arccos\frac{1}{\sqrt{3}}$	$-\arccos\frac{1}{\sqrt{3}}$	$\frac{\pi}{4}$	$-\arccos\frac{1}{\sqrt{3}}$
ϕ	$\frac{3\pi}{4}$	$\frac{3\pi}{4}$	$(0, \frac{\pi}{2})$ [b]	$\frac{3\pi}{4}$
χ	$\pi(1+\frac{2t}{T})$	$\pi(1+\frac{2t}{T})$	$\pi(1+\frac{t(4,8)}{T})$	$\pi(1+\frac{2t}{T})$
α	$(0, -\frac{\pi}{3})$	$(0, -\frac{\pi}{3})$	$(0, -\pi, 0, \frac{\pi}{2})$ [c]	$(0, -\pi)$

[a] SE: Spin Echo
[b] $(0, \frac{\pi}{2})$: $\phi = 0$, t $\in [0, \frac{T}{2}]$ and $\phi = \pi/2$, t $\in [\frac{T}{2}, T]$
[c] $(0, -\pi, 0, \frac{\pi}{2})$: $\phi = 0$, t $\in [0, \frac{T}{4}]$, $\phi = -\pi$, t $\in [\frac{T}{4}, \frac{T}{2}]$, $\phi = 0$, t $\in [\frac{T}{2}, \frac{3T}{4}]$ and $\phi = \pi/2$, t $\in [\frac{3T}{4}, T]$

Comparison of the robustness against the systemic error of Rabi frequency, i.e., the relative pulse deviation β, of all the four implementations are shown in Fig. 4. From the numerical result, we can clearly see that the NHQC+ scheme is more robust against the pulse control errors than the corresponding DG scheme, for both cases with and without spin echo. Therefore, we conclude that NHQC+ gate generally have better performance than DG gate under the same control strategy.

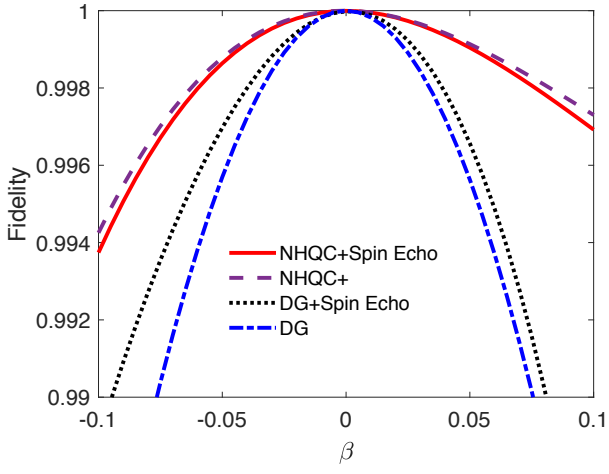

FIG. 4. The robustness of U_S gate against the systemic error of Rabi frequency, for different implementation methods of NHQC+ Spin Echo, NHQC+, DG+ Spin Echo and DG, without considering the relaxation.

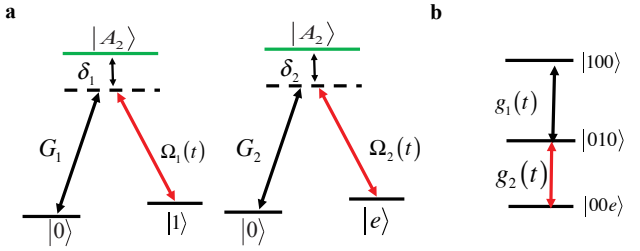

FIG. 5. (a) Illustration of physical realization of single and two-qubit gates in a solid-state NV center, for realizing two-qubit gate, two NV centers are coupled to a cavity in a two-photon Raman resonant way (b) Effective two-qubit couplings in one excited subspace.

II. TWO-QUBIT NHQC+ GATE

Additionally, we can further construct a nontrivial two-qubit controlled-phase (CP) gate, when the coupling between two NV centers is available. For example, let us consider the scenario of two NV centers coupled to a fused-silica microsphere optical cavity [18, 19] with a large detuning. The coupling configuration of a NV center for nontrivial two-qubit gates is shown in Fig. a, where the NV centers can be attached around the equator of the cavity, and the light-matter interaction G_j is induced via the evanescent field of the cavity mode [18], when the coupling between the two NV centers is mediated by a cavity in the Raman resonant regime, the effective Hamiltonian of the two-qubit gate becomes,

$$H_2(t) = g_1 a\sigma_1^+ + g_2 a\sigma_e^+ + \text{H.c.}, \tag{20}$$

where $a^\dagger(a)$ is the creation (annihilation) operator of the cavity, $\sigma_1^+ = |1\rangle\langle 0|$ and $\sigma_e^+ = |e\rangle\langle 0|$ are an electronic flip operator, and the effective cavity assisted coupling strength $g_j = G_j\Omega_j/\delta_j$ can be conveniently tuned via the amplitude of the corresponding external driven laser field Ω_j.

In this way, the Hamiltonian in Eq. (20) is equivalent to a resonant three-level system, working in the single excitation subspace $\{|100\rangle, |010\rangle, |00e\rangle\}$ of the coupled Hamiltonian,

$$H_3(t) = g_1(t)|100\rangle\langle 010| + g_2(t)|00e\rangle\langle 010| + \text{h.c.}, \tag{21}$$

where $|mnq\rangle \equiv |m\rangle_1|n\rangle_c|q\rangle_2$ with the subscript 1, 2 and c indicate the states belong to NV centers 1 and 2, and the cavity, shown in Fig. b. Note that there exists a dark eigenstate with zero eigenvalue, it can be written as: $|\mu_0(t)\rangle = \cos\mu(t)\cos\eta(t)|100\rangle + i\sin\mu(t)|010\rangle - \cos\mu(t)\sin\eta(t)|00e\rangle$, with the effective coupling strengths given by $g_1(t) = \dot{\eta}(t)\cot\mu(t)\sin\eta(t) - \dot{\mu}(t)\cos\eta(t)$ and $g_2(t) = \dot{\eta}(t)\cot\mu(t)\cos\eta(t) + \dot{\mu}(t)\sin\eta(t)$.

Subject to the boundary conditions: $\eta(0) = \eta(\tau) = 0$ and $\mu(0) = \mu(\tau) = 0(2\pi)$ for the cyclic evolution, there are many possible solutions to $\mu(t)$ and $\eta(t)$ for optimizing the time evolution. In particular, when the initial state is set as $|100\rangle$, after a cyclic evolution, the state $|100\rangle$ acquires a geometric phase γ, while the other states remain unchanged. In the computing space spanned by $\{|00\rangle, |01\rangle, |10\rangle, |11\rangle\}$, a holonomic CP gate can be expressed as

$$U_{CP}(\gamma) = diag(1, 1, 1, e^{i\gamma}), \tag{22}$$

where *diag* donates the diagonal matrix element. In general, the nontrivial two-qubit holonomic logical gate can be realized by controlling the γ, that is, adjusting the phase of one of the two steps similar to the realization of single qubit. In other words, we can achieve a universal set of holonomic gates for the NV-center system in the framework of NHQC+.

III. ROBUST PULSES WITH QUANTUM OPTIMAL CONTROL

Here, in order to construct the solution of time-dependent Schrödinger equation, we can combine the states $|\mu_+(t)\rangle$ with dynamical phase and geometric phase, i.e, $|\psi_+^0(t)\rangle = e^{if(t)}|\mu_+(t)\rangle$, with $f(t) = \int_0^t \langle\mu_+(t)|i\frac{\partial}{\partial t} - H(t)|\mu_+(t)\rangle dt$. Combining $|\mu_+^0(t)\rangle$ and the time-dependent Schrödinger equation, we find

$$f(t) = \int_0^t \frac{\Omega(t')\cos[\phi_1(t') - \alpha(t')]}{\sin\chi(t')}dt'. \tag{23}$$

Now, we need to inverse engineer the Hamiltonian with the evolution states. For achieving a cyclic evolution for GQC, we have the cyclic evolution condition $\chi(0) = \pi$ and $\chi(\tau) = 3\pi$. Then we get the Hamiltonian with help of Schördiger's equation and Eq. (23), i.e,

$$\begin{aligned}
\Omega(t) &= \sqrt{\dot{\chi}^2(t) + \dot{f}^2(t)\sin^2\chi(t)}\,, \\
\Delta(t) &= -\dot{f}(t)\cos\chi(t) - \dot{\alpha}(t)\,, \\
\phi_1(t) &= \alpha(t) + \arctan\left(\frac{\dot{\chi}(t)}{\dot{f}(t)\sin\chi(t)}\right).
\end{aligned} \tag{24}$$

Thus, we can solve the αt by choosing the parameters $\chi(t)$ and $\phi_1(t)$ according to the Eq. (24).

A. NHQC+DCGs

The pulses of dynamically corrected gates [21] are to resist decoherence, which the DCGs are tailored under the static noise model, usually by canceling the effect of noise on the evolution operator up to certain orders using piecewise constant pulses (PCP). In realistic situations, the DCGs should work well for the low frequency components of the noises but not high-frequency parts. The SUPDODE pulse [22, 23], a type of dynamically corrected gate, has been proposed to suppress the dephasing noise during quantum gates. The five-piece SUPCODE pulse has been used here, where the waiting time $\tau_{1(3)}$ and the pulse τ_2 duration satisfy the specific requirement, i.e., $[\tau_1 - \tau_2 - \tau_3 - \tau_2 - \tau_1]$, where $\tau_i (i = 1, 2, 3)$

are normalized time intervals given as follows,

$$\tau_1 = \csc\theta\left(2\cos^2\frac{\theta}{2} - 2\cos\frac{\theta}{2} + \sqrt{4 - 8\cos\frac{\theta}{2} + \cos\theta + \theta\sin\theta}\right),$$
$$\tau_2 = \theta/2\,,$$
$$\tau_3 = -2\left(\tau_1\cos\frac{\theta}{2} + \sin\frac{\theta}{2}\right). \quad (25)$$

Here, the axis in the equatorial, and the pulse is designed for $\theta \in (2\pi, 3\pi)$, which is equivalent to a gate operator $U(\theta_0)$ with $\theta_0 \in (0, \pi)$. For example, to realize a 0.5π pulse, θ is set to 2.5π. In our NHQC+, we apply the five-piece SUPCODE $\pi/2$ pulse twice for the case of π in the basis $\{|\Phi\rangle, |e\rangle\}$. For this purpose, we simply set $\alpha = 0$, $\phi_1 = \frac{\pi}{2}$ and $\chi = 2\pi t/\theta$. Under the five-piece SUPCODE pulse, the detuning error δ of holonomic gate can be cancelled up to second order of.

B. NHQC+Floquet Optimal Control

Pulse shaping based on variational calculus with Floquet theory yields [24, 25] various advantages that promise to improve our capabilities to control quantum systems. Here, we can combine our method with Floquet optimal control. The control pulses were optimized in an iterative fashion. For this purpose, a control pulse

$$s_{1(2)}(t) = \sum_{k=1}^{N} a_{1(2),k}\sin(kAt)\,. \quad (26)$$

is parametrized in terms of a small number (N) of Fourier components with fundamental frequency A and amplitudes $a_{1(2),k}$. In the present work, the case of NHQC+ in the three-level system controlled by a microwave pulse can be modelled by the Hamiltonian

$$H_s(t) = \frac{\Omega_0}{2}\sqrt{s_1^2(t) + s_2^2(t)}e^{-iB(t)}|\Phi\rangle\langle e| + H.c.\,, \quad (27)$$

where the time-dependent phase factor is defined as $B(t) = \arctan\left(\frac{s_2(t)}{s_1(t)}\right)$, and Ω_0 is relative control amplitude. As we target the implementation of pulses that work for holonomic gate with different parameters, the target functionals will always be averaged over these quantities. More explicitly, we used the target functionals

$$F = |\langle\psi_f|U(t_f)|\psi_i\rangle|^2 \quad (28)$$

where $|\psi_i\rangle$ and $|\psi_f\rangle$ denote the initial state and final target state. In order to maximize the target functionals, we choose the Fourier components which were given in the supplementary material of Ref.[25] as the Table III.

TABLE III. Optimal pulses with the control parameters $a_{1(2),k}$

pulse	parameters
$a_{1,1}, a_{1,2}, a_{1,3}, a_{1,4}, a_{1,5}$	-1.177, 1.646, -0.549, -1.668, -0.627
$a_{1,6}, a_{1,7}, a_{1,8}, a_{1,9}, a_{1,10}$	0.151, 1.680, -0.024, 0.858, 1.311
$a_{2,1}, a_{2,2}, a_{2,3}, a_{2,4}, a_{2,5}$	-0.150, -0.355, 0.253, 1.165, 0.069
$a_{2,6}, a_{2,7}, a_{2,8}, a_{2,9}, a_{2,10}$	0.470, -0.649, -0.814, 0.643, -0.657

* zyxue83@163.com
† x.wang@cityu.edu.hk
‡ yung@sustc.edu.cn

[1] D. Li, and M. H. Yung, New J. Phys. **16**, 053023 (2014).
[2] J. A. Jones, V. Vedral, A. Ekert, and G. Castagnoli, Nature **403**, 869 (2000).
[3] L. M. Duan, J. I. Cirac and P. Zoller, Science **292**, 1695 (2001).
[4] E. Sjöqvist, D. M. Tong, L. M. Andersson, B. Hessmo, M. Johansson, and K. Singh1, New J. Phys. **14**, 103035 (2012).
[5] G. F. Xu, J. Zhang, D. M. Tong, E. Sjöqvist, and L. C. Kwek, Phys. Rev. Lett. **109**, 170501 (2012).
[6] G. D. Chiara and G. M. Palma, Phys. Rev. Lett. **91**, 090404 (2003).
[7] P. J. Leek, J. M. Fink, A. Blais, R. Bianchetti, M. Göppl, J. M. Gambetta, D. I. Schuster, L. Frunzio, R. J. Schoelkopf, and A. Wallraff, Science **318**, 1889 (2007).
[8] S. Filipp, J. Klepp, Y. Hasegawa, C. Plonka-Spehr, U. Schmidt, P. Geltenbort, and H. Rauch, Phys. Rev. Lett. **102**, 030404 (2009).
[9] Wang, X. B., and M. Keiji, Phys. Rev. Lett. **87**, 097901 (2001).
[10] S.-L. Zhu, and Z. D. Wang, Phys. Rev. Lett. **89**, 097902 (2002).
[11] S.-L. Zhu, and Z. D. Wang, Phys. Rev A **67**, 022319 (2003).
[12] Z.-Y. Xue, F.-L. Gu, Z.-P. Hong, Z.-H. Yang, D.-W. Zhang, Y. Hu, and J. Q. You, Phys. Rev. Appl. **7**, 054022 (2017).
[13] J. T. Thomas, M. Lababidi, and M. Tian, Phys. Rev. A **84**, 042335 (2011).
[14] M. Johansson, E. Sjöqvist, L. M. Andersson, M. Ericsson, B. Hessmo, K. Singh, and D. M. Tong, Phys. Rev. A **86**, 062322 (2012).
[15] S. B. Zheng, C. P. Yang, and F. Nori, Phys. Rev. A **93**, 032313 (2016).
[16] J. Jing, C.-H. Lam, and L.-A. Wu, Phys. Rev. A **95**, 012334 (2017).
[17] H. R. Lewis, and W. B. Riesenfeld, J. Math. Phys. **10**, 1458 (1969).
[18] Y.-S. Park, A. K. Cook, and H. Wang, Nano. Lett. **6**, 2075 (2006).
[19] P. E. Barclaya, Kai-Mei C. Fu, C. Santori, and R. G. Beausoleil, Appl. Phys. Lett. **95**, 191115 (2009).
[20] A. Ruschhaupt, X. Chen, D. Alonso, and J. G. Muga, New. J. Phys. **14**, 093040 (2012).
[21] K. Khodjasteh, and L. Viola, Phys. Rev. Lett. **102**, 080501 (2009).
[22] X. Wang, L. S. Bishop, J. P. Kestner, E. Barnes, K. Sun, and S. D. Sarma, Nat. Commun. **3**, 997 (2012).
[23] X. Rong, J. Geng, F. Shi, Y. Liu, K. Xu, W. Ma, F. Kong, Z. Jiang, Y. Wu, and J. Du, Nat. Commun. **6** (2015).
[24] B. Bartels and F. Mintert, Phys. Rev. A **88**, 052315 (2013).
[25] T. Nöbauer, A. Angerer, B. Bartels, M. Trupke, S. Rotter, J. Schmiedmayer, F. Mintert, and J. Majer, Phys. Rev. Lett. **115**, 190801 (2015).